Metamorphic pressure–temperature conditions of garnet granulite from the Eastern Iratsu body in the Sambagawa belt, SW Japan

Daisuke NAKAMURA[*], Mutsuki AOYA[**] and Tomoki OKAMURA[***]

[*]*Faculty of Environmental, Life, Natural Science and Technology, Okayama University, Okayama 700–8530, Japan*
[**]*Graduate School of Technology, Industrial and Social Sciences, Tokushima University, Tokushima 770–8506, Japan*
[***]*Graduate School of Natural Science and Technology, Okayama University, Okayama 700–8530, Japan*

Several coarse–grained mafic bodies with evidence for eclogite–facies metamorphism are present in the Besshi area of the Sambagawa subduction–type metamorphic belt, SW Japan. Among them the granulite–bearing Eastern Iratsu metagabbro body involves an unresolved problem of whether it originated in the hanging–wall or footwall side of the subduction zone. The key to settle this problem is its relationship with the adjacent Western Iratsu metabasaltic body, which includes thick marble layer and certainly has the footwall ocean–floor origin. Several previous studies consider that the Western and Eastern Iratsu bodies were originally coherent in the footwall side and formed the shallower and deeper parts of a thick oceanic crust, respectively. The validity of this hypothesis may be assessed by deriving pressure–temperature history of the Eastern Iratsu body, or especially the pressure (depth) condition of the granulite–facies metamorphism before the eclogite–facies overprinting because, if the pressure was relatively high, the oceanic crust assumed in the above hypothesis might be too thick to tectonically achieve the present–day adjacence of the two bodies on the geological map. This study petrologically analyzes a garnet–bearing granulite from the Eastern Iratsu body and newly reports stable coexistence of garnet and orthopyroxene in the sample. By utilizing a garnet–orthopyroxene geothermobarometer, the minimum *P–T* conditions of the granulite–facies stage was estimated to be 0.8 GPa (~ 27 km in depth) and 780 °C. If the Western and Eastern Iratsu bodies were assumed to have formed a coherent oceanic crust before their subduction, the original thickness of it was >27 km and this demands unusually strong ductile shortening (<1/9) or unrealistically large vertical displacement on intraplate faulting, suggesting invalidity of the assumption. The Western and Eastern Iratsu bodies, therefore, are originally bounded by subduction–boundary fault and the obtained pressure of 0.8 GPa can be interpreted to represent that of the hanging–wall lower continental crust in the subduction zone, where the Eastern Iratsu body originated. After the granulite–facies metamorphism, the Western Iratsu body, which was located near the footwall surface, initiated subduction and was subsequently juxtaposed with the above–located Eastern Iratsu body at the corresponding depth (~ 27 km or greater) along the subduction boundary.

Keywords: Sambagawa belt, Iratsu body, Metagabbro, Granulite, Hanging wall

INTRODUCTION

In the Besshi area of the Sambagawa subduction–type metamorphic belt, SW Japan (Fig. 1a), several mafic bodies being coarser–grained than surrounding schists locally occur (Fig. 1b). These block–like bodies include the Tonaru (e.g., Miyagi and Takasu, 2005), Western Iratsu (e.g., Endo et al., 2009; Endo, 2010), Eastern Iratsu (e.g., Sakurai and Takasu, 2009), and Seba metagabbro bodies (e.g., Takasu, 1984; Aoya et al., 2006), and they commonly preserve petrological evidence for eclogite–facies metamorphism. These bodies were previously interpreted to be tectonic blocks which intruded into 'normal', or non–eclogitic, Sambagawa schists which directly surround them (e.g., Takasu, 1989). However, recent petrological and geological studies have revealed that presences of high–pressure rocks that underwent eclogite–facies metamorphism prior to the main Sambagawa metamorphism are not restricted to those tectonic blocks, but are more widely distributed in the eclogite–facies unit (Fig. 1b), a high–grade tectonic sheet which also includes eclo-

doi:10.2465/jmps.241001
D. Nakamura, nakadai@okayama-u.ac.jp Corresponding author

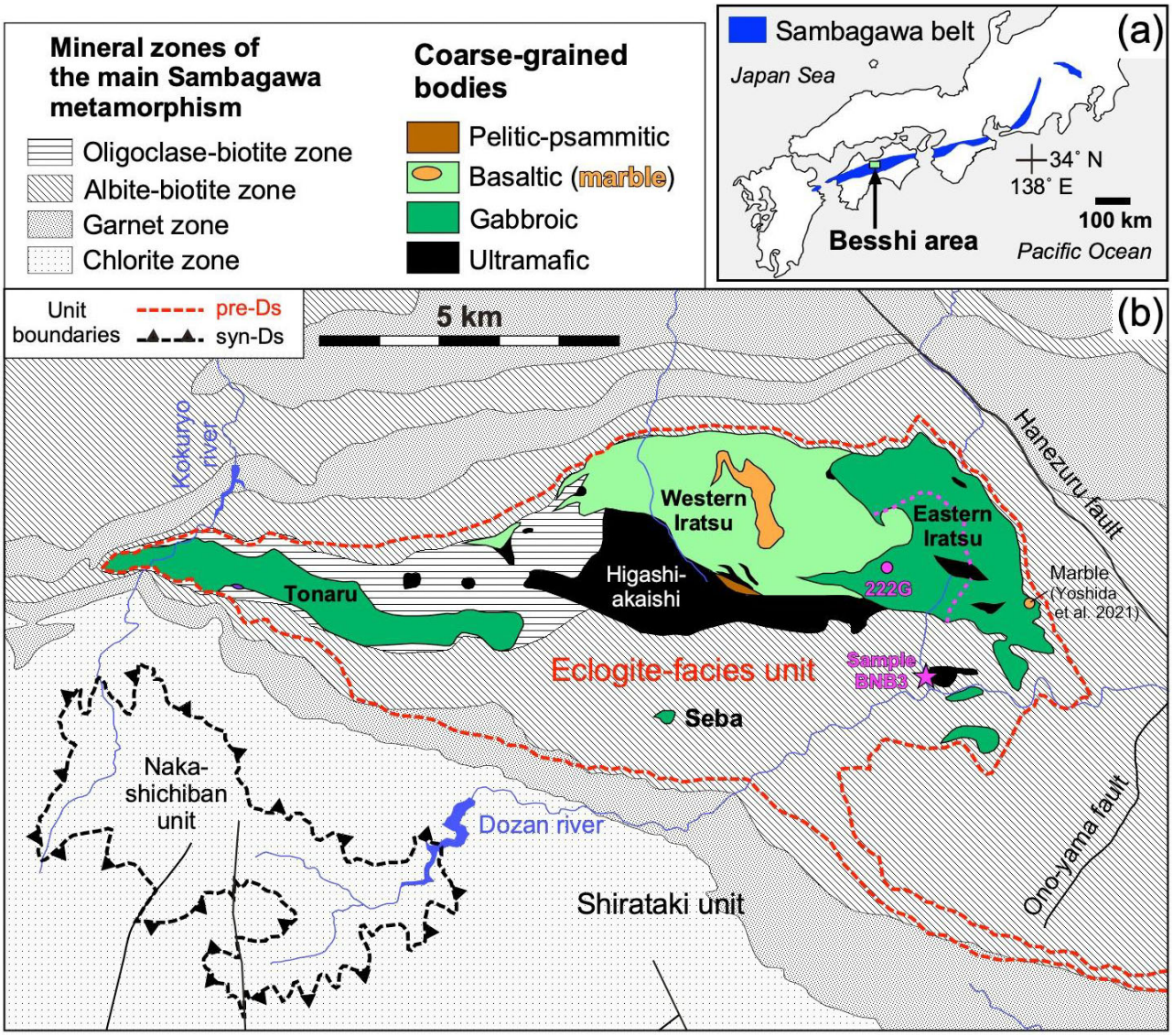

Figure 1. (a) Distribution of the Sambagawa metamorphic belt in SW Japan with locality of the Besshi area. (b) Metamorphic zonation map of the Besshi area with distributions of the coarse-grained mafic and ultramafic bodies based on Aoya et al. (2013b). Broken red line shows the boundary between the eclogite-facies and non-eclogitic (Shirataki and Nakashichiban) units. Ds: main deformation phase in the Sambagawa belt. Locality of the boulder sample for this study (BNB3) and of an outcrop granulite sample reported by Tanaka (1994) (222G) are shown by pink star and circle, respectively, as well as the Eastern-Iratsu marble analysed by Yoshida et al. (2021) (orange circle). The dotted pink line indicates a watershed of Nikubuchi-river system which corresponds to the outline of possible source region for BNB3 in the Easter Iratsu body.

gitic schists (e.g., Wallis and Aoya, 2000; Aoya, 2002; Aoki et al., 2009; Aoya et al., 2013a, 2013b; Kouketsu et al., 2014). Among the coarse-grained mafic bodies, evolution history of the Western Iratsu body have been best studied and there is a consensus that this body originated as ocean-floor basalt because it contains marble layers with thickness of several 10s of meters (Fig. 1b; Kugimiya and Takasu, 2002; Endo et al., 2012) and also pelitic-psammitic gneisses (Aoya et al., 2013b; Aoki et al., 2020b). In contrast, the origin of the adjacent and gabbroic Eastern Iratsu body remains to be an unresolved issue because this body contains relics of the older-stage granulite-facies metamorphism (e.g., Yokoyama, 1976; Goto and Banno, 1990; Tanaka, 1994). Thus, there is a problem of where the Eastern Iratsu body underwent the granulite-facies metamorphism before the high-pressure overprinting in the eclogite-facies (e.g., Endo and Tsuboi, 2013). One possible idea is that the Eastern Iratsu body was originally situated in the lower continental crust as a hanging wall of the subduction zone (e.g., Takasu, 1989) when the Western Iratsu body started its subduction from the trench at ~ 120 Ma (Endo et al., 2009; Aoki et al., 2020b). In this case, the Eastern Iratsu body was juxtaposed with the Western Iratsu body during the subduction of the latter,

and the resultant boundary between them should be tectonic. The other idea is that the Eastern Iratsu body was originally in the footwall side of the subduction zone, that is, in a deep part of thick oceanic crust (e.g., Ota et al., 2004; Terabayashi et al., 2005) or island arc (Utsunomiya et al., 2011; Aoki et al., 2020a, 2020b). In this case, the Western and Eastern Iratsu bodies are regarded to have already formed a single coherent unit before a common subduction metamorphism which initiated at ~ 120 Ma. A key to assess the validity of these hypotheses can be obtained from the pressure–temperature (*P*–*T*) history of the granulite-bearing Eastern Iratsu body if it is combined with the present spatially adjacent relationship with the Western Iratsu body (Fig. 1b). In this study, we report a newly found mafic (spinel-free) rock sample that preserves relic minerals of the granulite-facies metamorphism showing stable coexistence with garnet and describe its petrological characteristics. Based on these petrological data, we give constraints on the *P*–*T* history of the sample, especially focusing on the pressure condition (or depth) of the granulite-facies metamorphism and discuss the origin of the Eastern Iratsu body.

GEOLOGICAL OUTLINE

The Sambagawa belt is an intermediate- to high-*P*/*T* reginal metamorphic belt (see Endo et al., 2024 for detail) exposed along the southern side on Median Tectonic Line (MTL) from Kanto Mountains in central Japan to Saganoseki Peninsula of Kyushu in western Japan (Fig. 1a). The Besshi area in the Sambagawa metamorphic belt is situated in the central part of Shikoku Island. A number of detailed geological and petrological studies have been performed in this area (see Aoya and Endo, 2017, and references therein), and the constituent rocks are mainly pelitic and mafic schists with subordinate amounts of piemontite-bearing siliceous schist and serpentinized ultramafic rocks (e.g., Aoya et al., 2013a, 2013b). With increasing grade, the metamorphic conditions of the main Sambagawa metamorphism, which affects the whole of the belt, are from the pumpellyite-actinolite facies, through the greenschist-blueschist facies boundary, to the epidote amphibolite facies. This variation in metamorphic grade is represented as division into four mineral zones based on the mineral assemblages of pelitic rocks: i.e., chlorite, garnet, albite-biotite, and oligoclase-biotite zones in order of increasing metamorphic grade (Higashino, 1990; Aoya et al., 2013a, 2013b) (Fig. 1b). In the high-grade part within the albite-biotite to the oligoclase-biotite zones, coarse-grained mafic to ultramafic bodies such as the Tonaru, Higashi-akaishi, Western Iratsu, Eastern Iratsu, and Seba bodies occur as parts of the eclogite-facies unit (e.g., Aoya et al., 2013a, 2013b; Kouketsu et al., 2014). Note that all the eclogite-facies metamorphism recognized in the Sambagawa belt predates the main Sambagawa metamorphism which is reflected in the metamorphic zonation. Constituent rocks of the Eastern Iratsu body (Fig. 1b) are commonly associated with prominent cm- to meter-scale mafic-felsic banded structure and are generally interpreted to be metagabbro (e.g., Banno et al., 1976). The studied sample (BNB3) was collected in the southernmost part of Nikubuchi valley (Fig. 1b) as a boulder. The locality of sampling on a topographic map, presence of cm-scale mafic and felsic domains (Fig. 2) and inclusion of granulite-facies relic minerals all support that the source region of BNB3 is in the southwestern part of the Eastern Iratsu body. As an example, the outcrop locality of a similar garnet granulite sample, 222G, reported by Tanaka (1994) is also shown in Figure 1b.

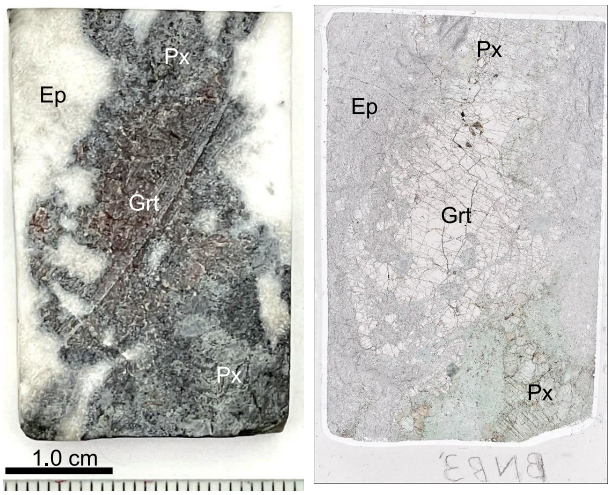

Figure 2. Photographs of a slab (left) and the thin section (right) of the studied sample (BNB3). Grt, garnet; Px, pyroxene; Ep, epidote.

PETROGRAPHY

The studied sample (BNB3) contains an extremely large garnet grain with the diameter exceeding 1.0 cm, which we refer to as garnet megacryst in this paper, and the matrix consists of white epidote-rich domains and dark-green pyroxene-rich domains (Fig. 2). Large or medium-sized grains (= 1–2 mm) of garnet and amphibole are present in the matrix of the pyroxene-rich domains. Orthopyroxene occurs as a matrix phase in the pyroxene-rich domain and as inclusions within the garnet megacryst and in the matrix clinopyroxene (Fig. 3), but it is absent from the epidote-rich domains. Sizes of orthopyroxene are approximately 1.0 mm in diameter in the matrix and less than 1.0 mm in garnet and clinopyroxene (Fig. 4). Orthopyroxene in-

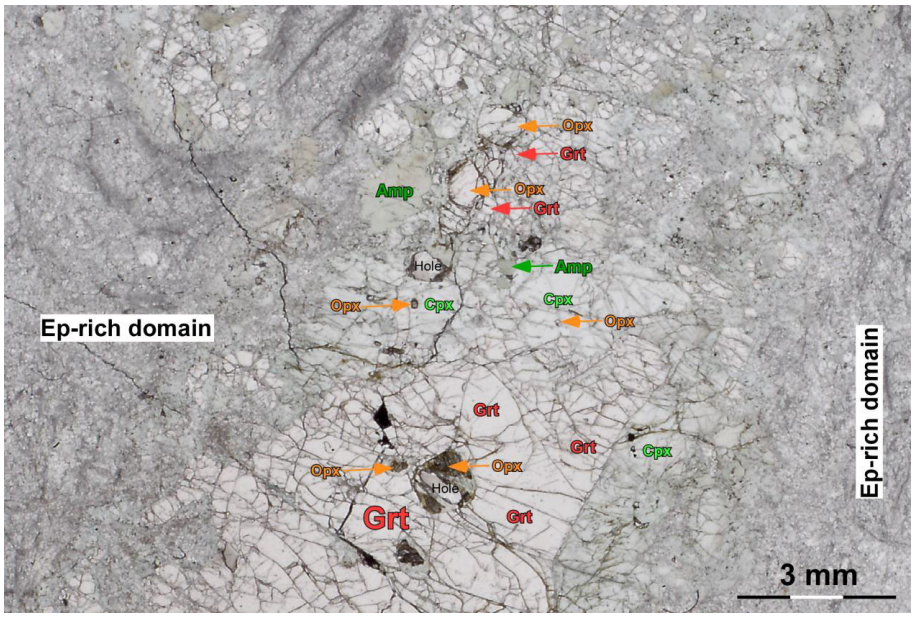

Figure 3. Scanned image of the orthopyroxene-bearing area in the studied thin section. Grt, garnet; Opx, orthopyroxene; Cpx, clinopyroxene; Amp, amphibole; Ep, epidote.

clusions in garnet are partially replaced by talc and amphibole. Clinopyroxene and amphibole inclusions are also present near the orthopyroxene inclusions in the garnet megacryst.

In the epidote-rich domains, medium-sized (~ 0.5 mm in length) and small (<0.15 mm) grains of kyanite sporadically occur, and they show needle-like shapes (Figs. 5 and 6). Small grains of quartz are also present in the epidote-rich domains, and they show irregular anhedral shapes (Figs. 5b and 6b). Medium-sized (~ 0.2 mm in length) amphibole grains are rare but present in these domains, and small grains (~ 0.02 mm in diameter) of omphacite develop around the amphibole grains (Figs. 5b and 6b). The omphacite grains are in contact with quartz. In addition, small amounts of Na-rich plagioclase and paragonite occur, and they are associated with quartz and kyanite (Figs. 5a and 6a).

MINERAL COMPOSITIONS

Chemical compositions of the constituent minerals were analyzed with an Electron Probe Micro Analyzer with four wave-length dispersive spectrometers, JEOL JXA8230, in Okayama University. Electron beam current and accelerating voltage were fixed to be 20 nA and 15 kV, respectively, and the beam diameter was set to be 3 μm. The peak and background counting times were set as 10 and 5 s, respectively, and the Bence and Albee correction procedure was employed. The selected standard materials are the same as written in Miyazaki et al. (2016). Mineral abbreviations and classification names of amphibole used in this paper follow those proposed by Whitney and Evans (2010) and Leake et al. (1997), respectively. Representative and main chemical compositions of the constituent minerals are listed in Tables 1 and 2.

Garnet

Garnet in the studied sample is very rich in pyrope component, and X_{Prp} [= Mg/(Fe + Mn + Mg + Ca)] ranges from 0.45 to 0.56 (Fig. 7). Ca contents are approximately constant, and X_{Grs} [= Ca/(Fe + Mn + Mg + Ca)] is within the range of 0.15-0.17 (Fig. 7). Such constant Ca contents in garnet can be explained by the coexistence of orthopyroxene, clinopyroxene and garnet. Thermodynamic calculations indicate that the Ca contents in garnet coexisting with orthopyroxene and clinopyroxene are mostly invariable regardless of the change in *P*-*T* conditions (e.g., Nakamura, 2003). Mn contents of the garnet are poor, and X_{Sps} [= Mn/(Fe + Mn + Mg + Ca)] is less than 0.02. The core part of the garnet megacryst is richer in Mg than the rim part of the grain, and the medium-sized grains of garnet in the matrix have approximately the same chemical compositions as the rim part of the garnet megacryst. A line profile of chemical compositions for a medium-sized garnet grain in the matrix was analyzed, and the compositions are nearly homogeneous except for the rim part where Fe content increases and Mg content decreases (Fig. 8). This garnet grain is in contact with orthopyroxene on the left side of it as shown in Figures 8 and 10.

Orthopyroxene

Orthopyroxene in the studied sample can be classified

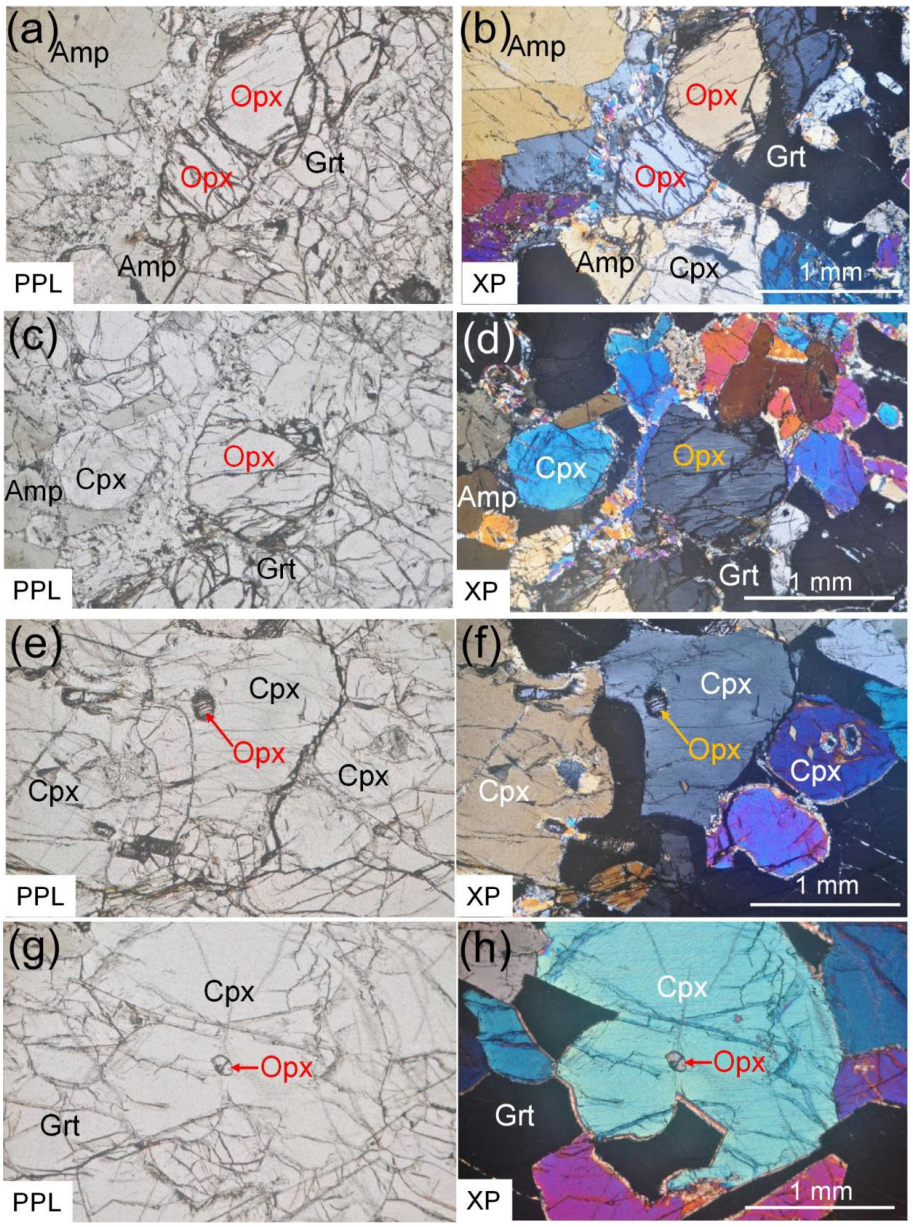

Figure 4. Photomicrographs of the studied thin section. (a) Orthopyroxene in the matrix. Plane-polarized light. (b) Cross-polars view of (a). (c) Orthopyroxene in the matrix. Plane-polarized light. (d) Cross-polars view of (c). (e) Orthopyroxene inclusion in clinopyroxene. Plane-polarized light. (f) Cross-polars view of (e). (g) Orthopyroxene inclusion in clinopyroxene. Plane-polarized light. (h) Cross-polars view of (g).

into three types based on the mode of the occurrences: i.e., inclusions in garnet, inclusions in clinopyroxene, and matrix grains. A clear difference in Mg# [= 100 Mg/(Mg + Fe^{2+})] between the inclusions in garnet and those in clinopyroxene was recognized (Fig. 9). The Mg# of the inclusions in garnet is higher (= 83.5–87.0) than that in clinopyroxene (= 80.0–82.5). In addition, Al and Si contents in orthopyroxene are different between the inclusions in garnet and those in clinopyroxene. The Al and Si contents in orthopyroxene inclusions in garnet tend to be poorer (Al = 0.140–0.162 apfu, based on O = 6) and richer (= 1.885–1.917 apfu) than those in clinopyroxene (Al = 0.156–0.205 apfu; Si = 1.875–1.909 apfu), respectively (Figs. 9a and 9b), indicating that Mg-tschermak component is relatively abundant in the inclusions in clinopyroxene compared with those in garnet. Ca contents are relatively constant regardless of the mode of the occurrences (Fig. 9c), except for a few data of the matrix orthopyroxene which has very thin lamellae (Fig. 4d). The matrix orthopyroxene grains have the intermediate compositions between the inclusions in garnet and those in clinopyroxene. Line profiles of chemical compositions for two matrix orthopyroxene grains were analyzed from A to B and from D to E (Fig. 10), and asymmetric chemical zonings were obtained from both grains (Fig. 11). The Al and Si contents decrease and increases toward the margins on the garnet-bearing side, respectively, indicating that Mg-tschermak component is poorer

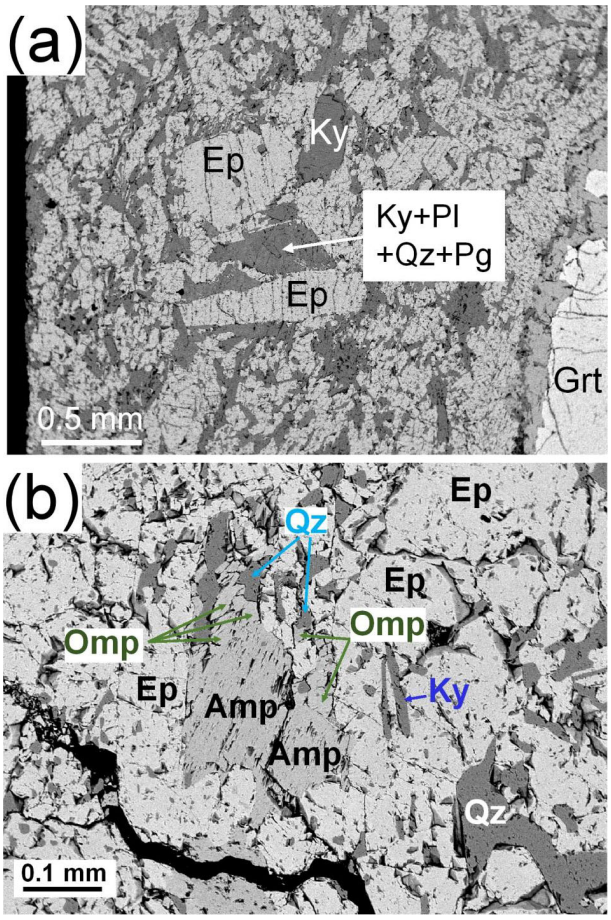

Figure 5. Back-scattered electron images of the epidote-rich domains. (a) Epidote and kyanite in the domains. Kyanite, plagioclase, quartz, and paragonite closely occurs in the small area. (b) Occurrence of small omphacite grains in the domain. Omphacite occurs around amphibole and is in contact with quartz. Ep, epidote; Ky, kyanite; Pl, plagioclase; Qz, quartz; Pg, paragonite; Grt, garnet; Omp, omphacite; Amp, amphibole.

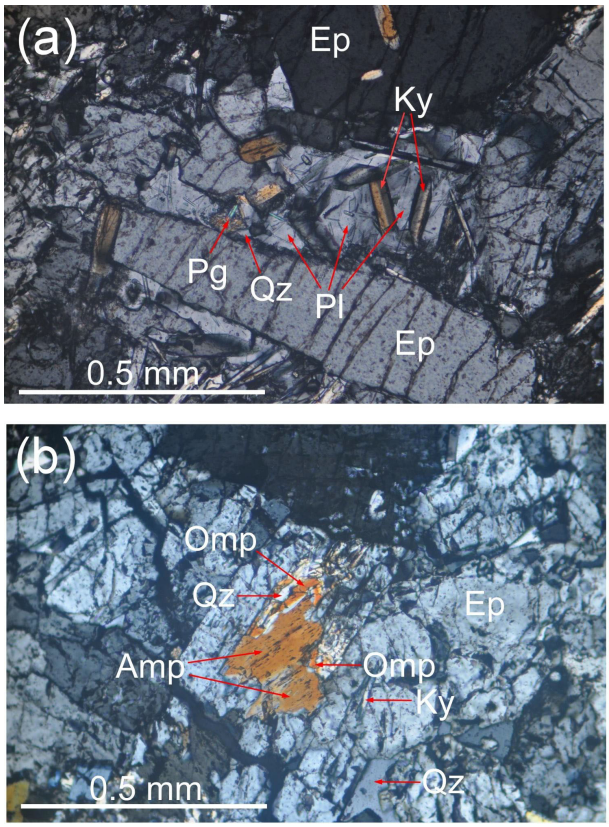

Figure 6. Photomicrographs (cross-polars views) of the epidote-rich domains. (a) Twined kyanite developing in albite-rich plagioclase. Small paragonite flakes with pale-blue interference color are present near a quartz grain. (b) Small omphacite with orange interference color developing around amphibole with similar orange interference color. Irregular-shaped quartz grains are present and in contact with omphacite. Mineral abbreviations are the same as those in Figure 5.

on the garnet-bearing side than the other side. Fe/Mg ratios do not significantly vary in the matrix orthopyroxene, although Fe contents in the neighboring garnet slightly increase at the rim (Fig. 8).

Clinopyroxene

Clinopyroxene is present both as the matrix grains and as inclusions in garnet. Na contents of them are approximately constant and low in the range of Na/(Na + Ca) = 0.058–0.105, and Mg# of them varies from 86.3 to 96.6 and does not differ between them (Fig. 12). Si contents of the inclusions in garnet tend to be richer (= 1.866–1.943 apfu, based on O = 6) than the matrix grains (= 1.837–1.900 apfu) (Fig. 12a). The matrix clinopyroxene grains near the garnet megacryst are relatively large (~ 1.8 mm in diameter), and they are nearly homogenous in chemical compositions (Si ~ 1.85; Mg# ~ 90) but show slight zonation with decreasing of Ca-tschermak content and increasing of Mg# toward their margins (Si ~ 1.90; Mg# ~ 96). Besides, very small grains of omphacite occur around amphibole in the epidote-rich domain (Figs. 5b and 6b). Na/(Na + Ca) of them is in the range from 0.438 to 0.578, and their Si contents are 1.936–1.967 apfu, based on O = 6 (Fig. 12).

Amphibole

In the matrix, amphibole occurs not only in the pyroxene-rich domains (Fig. 3) but also in the epidote-rich domains (Figs. 5b and 6b). In addition, amphibole is present both as these matrix grains and as inclusions in garnet and clinopyroxene. Furthermore, retrograde products of amphibole develop along the grain boundaries in the pyroxene-rich domains (Fig. 10). Other retrograde amphibole products occur as replacing orthopyroxene inclusions in garnet.

Table 1. Representative and major chemical compositions of garnet, orthopyroxene, and clinopyroxene of the studied sample

Minerals	Grt1 Core In matrix	Grt2 Core Megacryst	Opx1 Near Grt1 In matrix	Opx2 Core In matrix	Opx3 Core In Grt	Opx4 Core In Cpx	Cpx1 Core In Grt	Cpx2 Core In matrix	Cpx3 Core Ep-rich d
SiO_2	41.17	41.22	54.27	53.23	53.89	53.14	51.90	51.17	55.46
TiO_2	0.02	0.06	0.02	0.05	0.04	0.02	0.28	0.23	0.08
Al_2O_3	22.80	23.18	3.74	5.07	3.93	4.55	5.23	6.51	11.24
Cr_2O_3	0.01	0.02	0.01	0.01	0.00	0.00	0.02	0.01	0.02
FeO*	15.62	14.59	11.91	12.11	10.74	13.03	4.71	4.68	4.24
MnO	0.37	0.44	0.09	0.12	0.16	0.16	0.04	0.06	0.10
MgO	14.49	15.14	30.07	29.10	30.98	28.86	14.41	13.79	9.24
CaO	5.85	5.88	0.26	0.44	0.46	0.29	22.83	23.08	14.22
Na_2O	0.02	0.01	0.01	0.03	0.01	0.02	1.24	1.00	6.71
K_2O	0.01	0.00	0.01	0.01	0.00	0.01	0.00	0.01	0.02
Total	100.35	100.53	100.40	100.16	100.20	100.08	100.64	100.52	101.33
O=	12	12	6	6	6	6	6	6	6
Si	3.013	2.998	1.906	1.878	1.885	1.882	1.877	1.857	1.938
Ti	0.001	0.003	0.001	0.001	0.001	0.001	0.008	0.006	0.002
Al	1.967	1.987	0.155	0.211	0.162	0.190	0.223	0.278	0.463
Cr	0.000	0.001	0.000	0.000	0.000	0.000	0.000	0.000	0.000
Fe^{3+}	–	–	0.033	0.033	0.066	0.046	0.094	0.066	0.111
Fe^{2+}	0.956	0.887	0.317	0.324	0.248	0.340	0.048	0.076	0.013
Fe(total)	0.956	0.887	0.350	0.357	0.314	0.386	0.142	0.142	0.124
Mn	0.023	0.027	0.003	0.004	0.005	0.005	0.001	0.002	0.003
Mg	1.581	1.641	1.575	1.530	1.615	1.524	0.777	0.746	0.481
Ca	0.459	0.458	0.010	0.017	0.017	0.011	0.885	0.897	0.532
Na	0.003	0.002	0.001	0.002	0.000	0.001	0.087	0.071	0.454
K	0.001	0.000	0.000	0.000	0.000	0.001	0.000	0.000	0.001
Total	8.004	8.006	4.000	4.000	4.000	4.000	4.000	4.000	4.000

*Total iron is written as FeO in weight percentage.

Compositions of Grt1 and Opx1 were used for *P–T* estimations of the granulite-facies stage. Those of Grt2 and Opx2 were used for the protolith *P–T* estimations. 'Ep-rich d' represents Ep-rich domain. Ferric iron contents in garnet are not calculated here. Ferric/ferrous ratios in Opx and Cpx are calculated with total cations = 4.

Thus, various types of amphiboles are present in the studied thin section, and they were formed during various stages of metamorphism. The amphibole inclusions are poor in Na(B) (<0.22 apfu, based on O = 23) and relatively rich in Na(A) (0.17–0.50 apfu), mainly classified as tschermakite. Large or medium-sized grains (= 1–2 mm) of amphibole in the pyroxene-rich domains of the matrix have similar Na(B) values to the amphibole inclusions but have slightly higher Na(A) values than the inclusions (Fig. 13), mostly classified as pargasite. These amphibole grains are classified as Ca amphibole. On the other hand, medium-sized grains (= 0.1–0.2 mm) of matrix amphibole in the epidote-rich domains show high Na(B) values, and nearly half of them is classified as Na-Ca amphibole (i.e., barroisite). Retrograde products of amphibole are relatively poor in Na(A) and Na(B) and rich in Si (up to 7.5 apfu), mainly classified as Mg-hornblende. Compared to large grains in pyroxene-rich domains, amphibole replacing orthopyroxene inclusions is slightly poor in Na(A) but relatively rich in Na(B) (Fig. 13). All analyzed amphibole data show higher Mg# than approximately 80.

Other minerals

Plagioclase is present in the epidote-rich domains (Figs. 5a and 6a), and its chemical compositions are from almost pure albite to oligoclase {X_{An} [= Ca/(Ca + Na + K)] = 0.01–0.15}. Two epidote-group minerals were recognized on the back-scattered electron images in the epidote-rich domains. Dark one has Fe^{3+}-poor compositions of X_{Ep} [= $Fe^{3+}/(Fe^{3+} + Al-2)$] = 0.059–0.094, and relatively bright one has Fe^{3+}-rich compositions of X_{Ep} = 0.414–0.452. In the pyroxene-rich domains, epidote occurs as reaction zones between quartz inclusions in clinopyroxene and the host phase. The epidote in clinopyroxene has compositions of X_{Ep} = 0.182–0.394. Small grains of paragonite

Table 2. Major chemical compositions of Amp, Ep, Pl, and Pg of the studied sample

Minerals	Amp Core Ep d	Amp Core Px d	Amp Core Inc	Amp Core Retro	Ep1 Core Ep- d	Ep2 Core Ep d	Ep3 Core Px d	Pl Core Ep d	Pg Core Ep d
SiO_2	49.23	43.09	44.17	54.26	39.73	38.88	39.23	69.48	48.04
TiO_2	0.23	0.80	0.62	0.11	0.01	0.11	0.04	0.00	0.01
Al_2O_3	12.59	16.36	15.05	5.22	33.09	28.01	29.76	20.18	40.13
Cr_2O_3	0.01	0.00	0.02	0.01	0.00	0.00	0.00	0.01	0.00
Fe_2O_3	-	-	-	-	1.39	7.79	5.38	-	-
FeO*	5.83	7.32	8.53	4.02	-	-	-	0.04	0.13
MnO	0.09	0.05	0.00	0.01	0.03	0.03	0.00	0.01	0.00
MgO	16.85	14.70	15.17	21.20	0.04	0.13	0.11	0.00	0.07
CaO	9.47	12.35	11.81	12.45	24.61	23.72	24.02	0.36	0.20
Na_2O	3.64	2.51	2.08	1.18	0.00	0.00	0.02	11.62	6.54
K_2O	0.43	1.48	0.64	0.01	0.00	0.00	0.00	0.03	1.32
Total	98.36	98.66	98.09	98.48	98.89	98.68	98.55	101.73	96.43
O=	23	23	23	23	12.5	12.5	12.5	8	11
Si	6.786	6.153	6.233	7.387	2.992	3.002	3.006	2.982	3.026
Ti	0.024	0.086	0.066	0.012	0.000	0.007	0.003	0.000	0.000
Al	2.045	2.753	2.502	0.838	2.937	2.549	2.688	1.021	2.980
Cr	0.001	0.000	0.002	0.001	0.000	0.000	0.000	0.000	0.000
Fe^{3+}	0.489	0.025	0.642	0.419	0.079	0.453	0.310	-	-
Fe^{2+}	0.182	0.849	0.364	0.039	-	-	-	-	-
Fe(total)	0.672	0.874	1.006	0.458	0.079	0.453	0.310	0.002	0.007
Mn	0.010	0.007	0.000	0.001	0.002	0.002	0.000	0.000	0.000
Mg	3.463	3.128	3.191	4.303	0.005	0.015	0.012	0.000	0.006
Ca	1.398	1.890	1.786	1.816	1.986	1.963	1.972	0.017	0.013
Na	0.974	0.695	0.569	0.311	0.000	0.000	0.003	0.967	0.799
K	0.076	0.270	0.115	0.002	0.000	0.000	0.000	0.001	0.106
Total	15.448	15.855	15.470	15.129	8.000	7.991	7.994	4.991	6.937

*For amphibole, plagioclase, and paragonite, total iron is written as FeO in weight percentage.
'Ep d' and 'Px d' represent epidote-rich and pyroxene-rich domains, respectively. 'Inc' and 'Retro' represent inclusion in clinopyroxene and retrograde product, respectively. Total iron in epidote is assumed to be ferric. Ferric/ferrous ratios in amphibole are calculated with total cations = 13 exclusive of K, Na, and Ca, and those in plagioclase and paragonite are not calculated here.

occur in the epidote-rich domains, and they are closely associated with kyanite, plagioclase, and quartz. The paragonite includes significant amounts of K (= 0.11-0.16 apfu, based on O = 11), and a thin lamella of phengitic mica (Si ~ 3.18 apfu, based on O = 11) exists in the paragonite.

DISCUSSION

P-T conditions of the granulite-facies stage

The pyroxene-rich domains preserve medium-sized grains of orthopyroxene in the matrix, and they are in contact with garnet (Figs. 4a-4d and 10). Therefore, we utilize a conventional garnet-orthopyroxene geothermobarometer in this study for the *P-T* estimation. Those orthopyroxene grains, however, have asymmetric chemical zonings, and Mg-tschermak ($MgAl_2SiO_6$) contents decrease toward the garnet-bearing side (Fig. 11). These asymmetric zonings of orthopyroxene probably represent that Al-poor chemical compositions near the garnet were equilibrated with garnet although the Al-rich opposite side of the orthopyroxene was not in equilibrium with the garnet. In addition, orthopyroxene inclusions in clinopyroxene are isolated by the host phase from garnet (Figs. 4e-4h), and they are rich in Al and clearly different in Al content from the garnet side of the orthopyroxene in the matrix (Fig. 9b), supporting the idea that the Al-rich parts of orthopyroxene were not in equilibrium with the garnet at the matrix formation stage. On the other hand, the garnet grain in contact with orthopyroxene is nearly homogenous except for a narrow area (<0.05 mm) of the rim where Fe contents increase, and Mg contents decrease (Fig. 8). The slight chemical modification of the narrow range of the rim can be interpreted to be due to the element exchange between the gar-

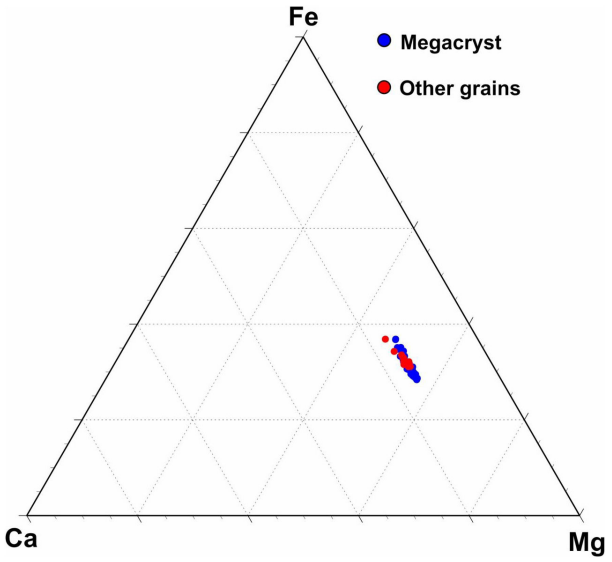

Figure 7. Fe–Mg–Ca triangle diagram showing garnet compositions in the studied sample.

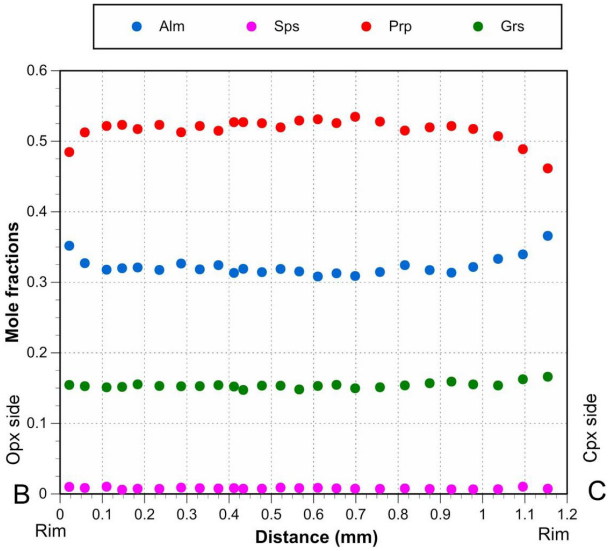

Figure 8. Garnet compositional profile from the point B to the point C in Figure 10. This grain is in contact with orthopyroxene on the left side and clinopyroxene on the right side. Alm, almandine; Sps, spessartine; Prp, pyrope; Grs, grossular.

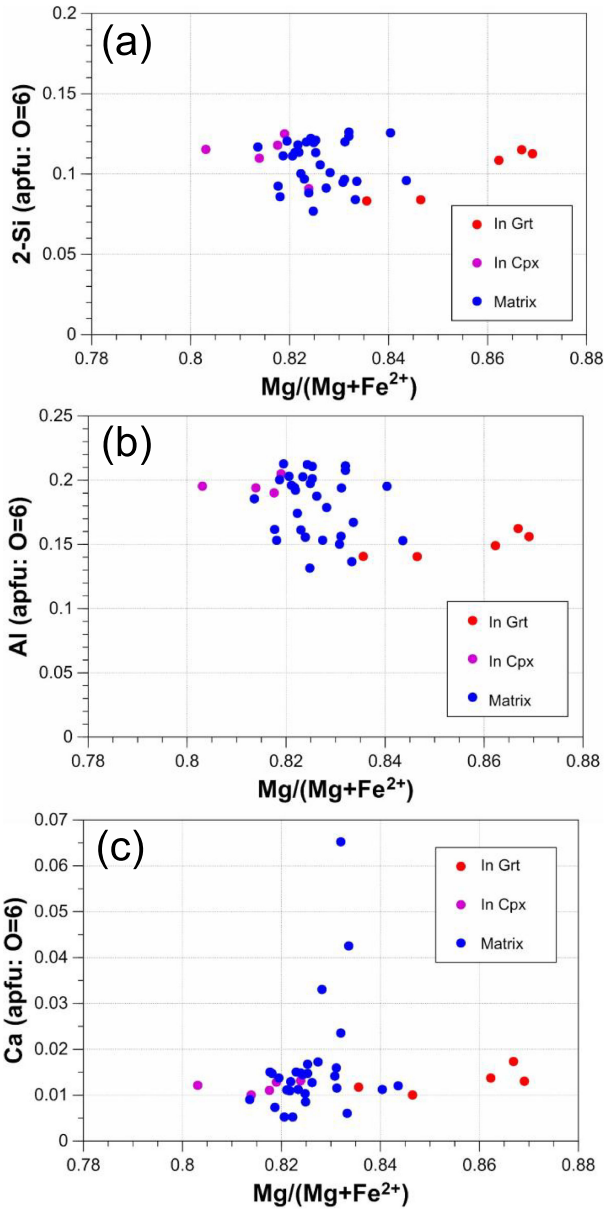

Figure 9. Orthopyroxene compositions of the studied sample. Fe^{2+} contents were calculated by making oxygen number be equal to 6 based on total cations number = 4.

net and the orthopyroxene at a later low-*T* stage. Thereby, Fe/Mg ratio of the orthopyroxene should have slightly decreased during the cooling stage, but Fe/Mg values of orthopyroxene do not significantly change along the analyzed lines (Fig. 11). Even if the orthopyroxene compositions were modified during the cooling, its chemical modification of orthopyroxene makes temperature calculated by the Fe–Mg exchange geothermometer lower than the actual granulite-facies metamorphic temperature. Thus, the actual temperature can be slightly higher than that calculated by this study. The garnet–orthopyroxene geobarometry shows a positive slope of the equilibrium line in the *P*–*T* diagram, and hence the calculated pressure should increase with increasing of the corresponding temperature.

In this study, the *P*–*T* conditions were calculated by using the average composition of four data from the Al-poor garnet side of orthopyroxene (Fig. 11a) in conjunction with the average composition of the adjacent garnet excluding the rim data. The Fe–Mg exchange garnet–orthopyroxene geothermometer calibrated by Harley (1984), in which the thermometer formulation was constructed by performing direct Fe–Mg exchange experi-

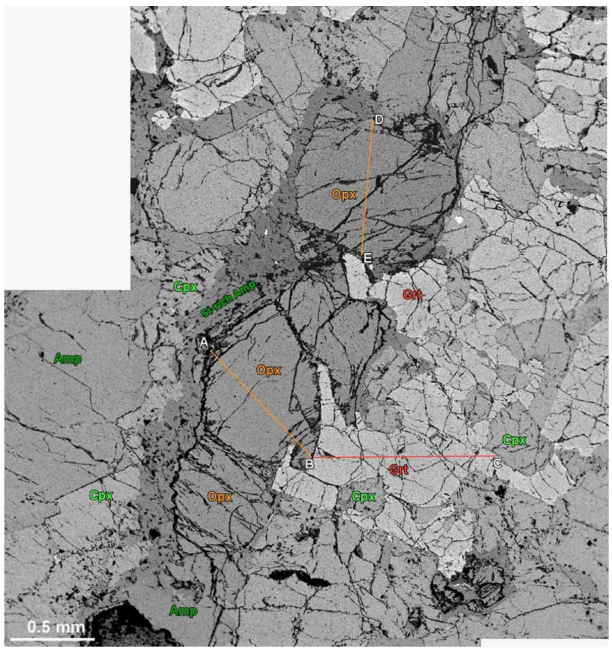

Figure 10. Back-scattered electron image of an orthopyroxene-bearing area in the matrix. Grt, garnet; Opx, orthopyroxene; Cpx, clinopyroxene; Amp, amphibole.

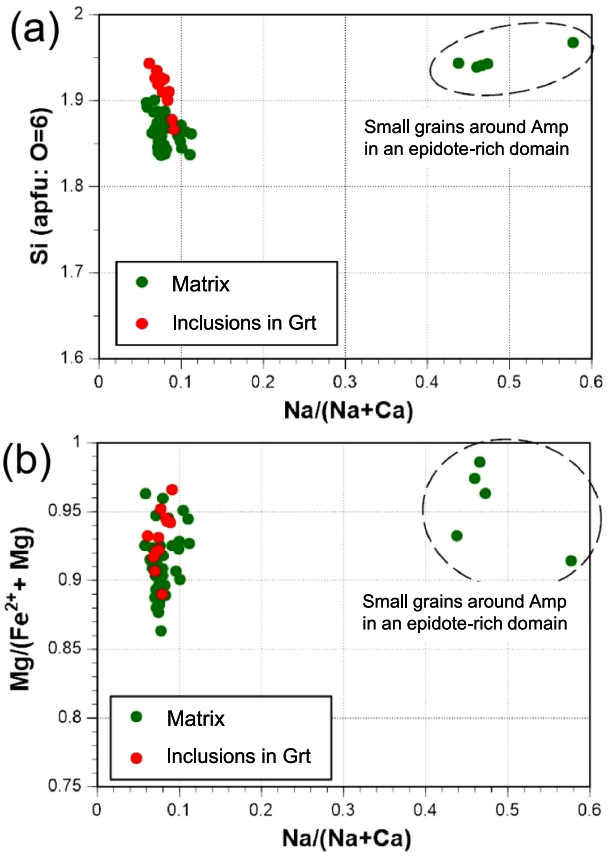

Figure 12. Chemical compositions of clinopyroxene in the studied sample. Fe^{2+} contents were calculated by making oxygen number be equal to 6 based on total cations number = 4.

ments in *P*-*T* conditions of 0.5-3.0 GPa and 800-1200 °C, and the garnet-orthopyroxene geobarometer based on a reaction of enstatite + Mg-tschermak = pyrope calibrated by Harley and Green (1982) were adopted for the *P*-*T* estimation. The calculation gave the *P*-*T* conditions of approximately 0.8 GPa and 780 °C (Fig. 14), which represents the minimum *P*-*T* conditions of the granulite-facies metamorphic stage in the studied sample. A tentative application of other garnet-orthopyroxene geothermometer formulations (Sen and Bhattacharya, 1984; Lee and Ganguly, 1988) to the same pair gave 842 and 898 °C at 0.8 GPa and 879 and 928 °C at 1.3 GPa, respectively, which are significantly higher than the temperatures estimated with the formulation of Harley (1984).

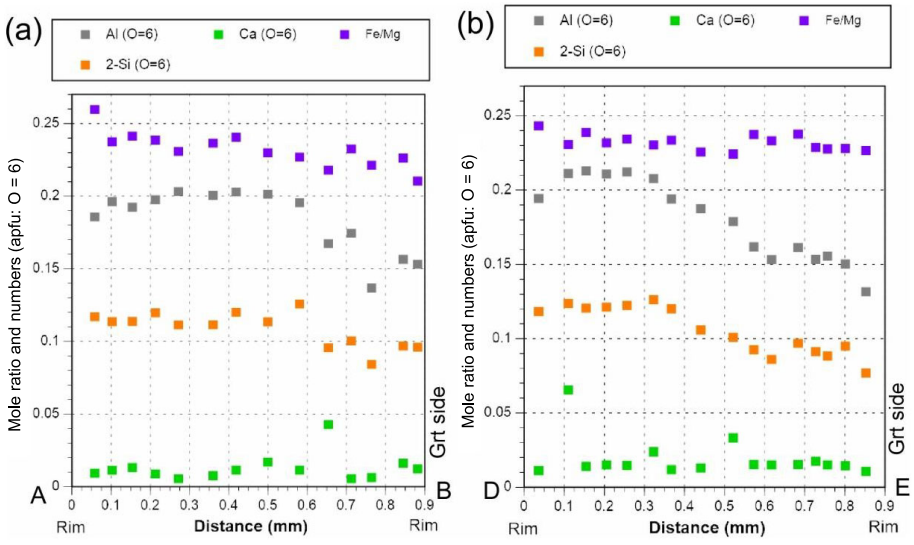

Figure 11. Orthopyroxene compositional profiles of the studied sample. (a) A profile from the point A to the point B shown in Figure 10. (B) A profile from the point D to the point E shown in Figure 10. Both orthopyroxene grains are in contact with garnet on the right side.

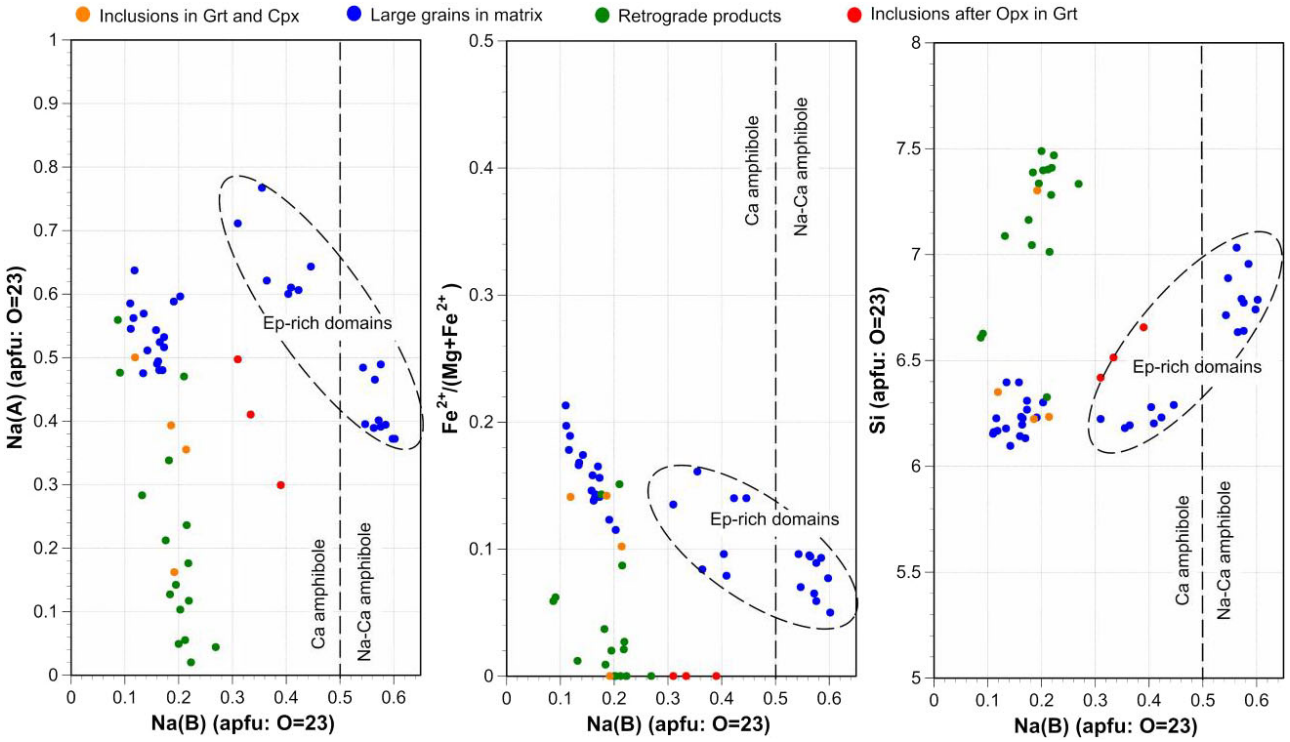

Figure 13. Chemical compositions of amphibole in the studied sample. Fe^{2+} contents were calculated by making oxygen number be equal to 23 based on Si + Ti + Cr + Al + Fe + Mn + Mg = 13. Grt, garnet; Cpx, clinopyroxene; Opx, orthopyroxene; Ep, epidote.

Thus, the above *P*–*T* conditions (0.8 GPa and 780 °C) can be judged to be the minimum *P*–*T* limits for the granulite-facies stage if we ignore errors of each formulation for the geothermobarometer. Besides, use of the average composition of four data from the Al-rich part of the matrix orthopyroxene and the Mg-rich core composition of the garnet megacryst gave *P*–*T* conditions of 0.8 GPa and 870 °C (Fig. 14), which may reflect older and higher-*T* conditions closely after the protolith formation stage if the Al-rich part of orthopyroxene preserves the original composition. Yokoyama (1980) estimated temperatures at the granulite-facies stage of ultramafic (spinel-bearing) rocks from the Nikubuchi body enclosed in the Eastern Iratsu body as 750 °C, which is slightly low but nearly consistent with our estimated minimum value (780 °C). Furthermore, Yokoyama (1980) estimated pressures at the granulite-facies stage as 0.5 to 1.0 GPa by using the stability of mineral assemblage of spinel + orthopyroxene + clinopyroxene + anorthite. Our estimated pressure (0.8 GPa) is also within the range of his estimation (0.5–1.0 GPa), but our pressure value (0.8 GPa) would be the minimum pressure limit of the granulite-facies stage as described in the above discussion: i.e., the actual granulite-facies pressure would have been higher than this value.

Eclogite-facies overprinting

The epidote-rich domains, which can be interpreted to be originally Ca-rich plagioclase, mainly consist of epidote and kyanite with small amounts of quartz, Na-rich plagioclase, paragonite, amphibole, and lesser omphacite. Epidote occurs mainly as relatively large grains, and kyanite occurs as both large and small grains (e.g., Figs. 5a and 6a). Small grains of Na-rich plagioclase, kyanite, paragonite, and quartz closely occur and create small areas in the epidote-rich domains (Fig. 6a). After the protolith formation and the subsequent granulite-facies stages, further refrigeration should have occurred and caused decomposition of the Ca-rich plagioclase to form epidote, kyanite, and small amounts of above phases. The formation of relatively large epidote and kyanite grains can be explained by a reaction, anorthite + H_2O = zoisite + kyanite + quartz, in the CaO–Al_2O_3–SiO_2–H_2O model system during the refrigeration (Fig. 14). Actually, however, Na_2O also should have been present in the original plagioclase, which probably caused the formation of small amounts of Na-rich plagioclase, paragonite, and Na-Ca amphibole. This assemblage together with epidote is characteristic of the high-*P* end of epidote-amphibolite facies (Konzett and Hoinkes, 1996; Molina and Poli, 1998) and these products were probably formed in the epidote-amphibolite facies as

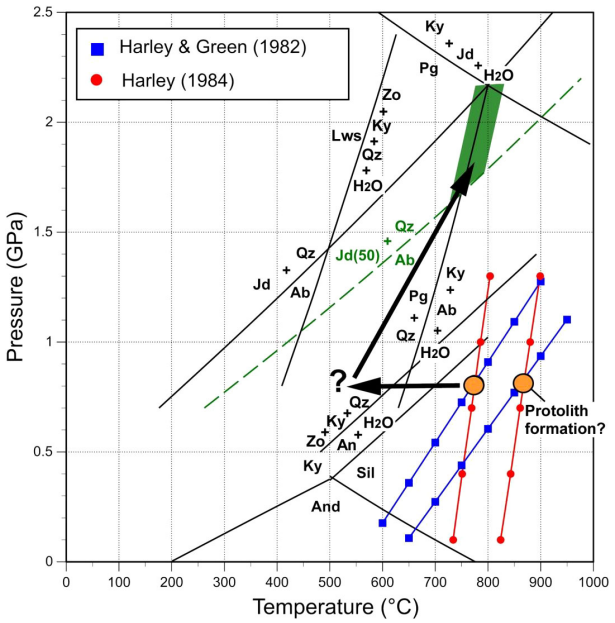

Figure 14. *P–T* conditions of protolith-formation, granulite-facies, and eclogite-facies stages of the studied sample. The *P–T* conditions of the protolith-formation and the granulite-facies stages were estimated with the garnet-orthopyroxene geothermobarometry (Harley and Green, 1982; Harley, 1984). The other reaction *P–T* curves were calculated with THERMOCALC v3.21 based on data of Holland and Powell (1998) (modified in 2002). Jd(50) represents that activity of jadeite component was fixed as 0.50. Ky, kyanite; Jd, jadeite; Pg, paragonite; Qz, quartz; Ab, albite; An, anorthite; Zo, zoisite; Lws, lawsonite; Sil, sillimanite; And, andalusite.

is also recognized for the earlier pre-eclogitic subduction metamorphism of the Western Iratsu body (Endo et al., 2009), the corresponding *P–T* conditions being from 0.9 GPa, 570 °C to 1.2 GPa, 660 °C (Endo et al., 2012). In addition, the presence of omphacite in contact with quartz around Na-Ca amphibole in the epidote-rich domains (Figs. 5b and 6b) further indicates that the eclogite-facies overprinting occurred after the epidote amphibolite-facies stage. The coexistence of omphacite and quartz in a plagioclase-absent small area such as Figures 5b and 6b can give a constraint to the minimum pressure of the eclogite-facies stage by a reaction of jadeite (in omphacite) + quartz = albite. The jadeite content in omphacite is approximately 50 mole% (Fig. 12). If we adopt a pseudo-ideal single-site solution model (e.g., Wood et al., 1980) for omphacite, activity of jadeite component in the omphacite becomes 0.5 and the minimum pressure limit for the stability of the omphacite + quartz association becomes approximately 1.6 GPa at 700 °C (Fig. 14). On the other hand, in other small areas with different effective bulk-rock compositions, the maximum pressure limit of the eclogite-facies stage can be constrained by the stability of albite against jadeite + quartz, because almost pure albite is locally preserved in the epidote-rich domains of this sample as observed in Figures 5a and 6a (Fig. 14). The stability of paragonite within some small areas in the epidote-rich domains against jadeite + kyanite provides another constraint on the maximum pressure (Fig. 14). In addition, an assemblage of kyanite + albite + quartz + paragonite observed within small areas in the epidote-rich domains (Figs. 5a and 6a) suggests that the temperature conditions from the epidote amphibolite-facies to eclogite-facies stage were probably located along or near a *P–T* curve for the reaction of paragonite + quartz = kyanite + albite + H_2O (Fig. 14). Thus, the *P–T* conditions of the eclogite-facies stage are roughly estimated to be 1.7-2.2 GPa, 750-800 °C. The reaction *P–T* curves drawn in Figure 14 were calculated with THERMOCALC v3.21 based on thermodynamic data of Holland and Powell (1998) (modified in 2002).

Origin of the Eastern Iratsu body

The consensus of previous studies is that the thick and mappable marble layer within the Western Iratsu body (Fig. 1b) originated as sedimentary limestone on a shallow part of ocean-floor, and the initial pressure condition should have been nearly equal to the atmospheric pressure (~ 10^{-4} GPa) + seawater pressure (~ 0.01 GPa if the seafloor was at 1-km depth beneath the sea surface). In contrast, as written in the above section, pressure condition of the granulite-facies stage of the Eastern Iratsu body was estimated to be 0.8 GPa, which corresponds to depth of about 27 km beneath the surface if we assume that the overlying rocks are basaltic and with the density of 3.0 g/cm^3 (34 km/GPa: e.g., Spear, 1993). On the other hand, the present-day distance between the Western-Iratsu marble and the studied granulite sample is only about 3 km at the most (Fig. 1b). Based on this change of the distance between the Western-Iratsu marble and the studied granulite sample, we will discuss the origin of the Eastern Iratsu body, i.e., in footwall side or hanging-wall side. Several previous studies consider the Western and Eastern Iratsu bodies formed together a thick oceanic crust in the footwall side before their subduction metamorphism (Ota et al., 2004; Terabayashi et al., 2005; Utsunomiya et al., 2011; Aoki et al., 2020a, 2020b) which initiated at ~ 120 Ma (Endo et al., 2009; Aoki et al., 2020b). In this interpretation, the marble of the Western Iratsu body represents the shallowest member of the oceanic crust while the granulite of the Eastern Iratsu body one of the deepest members of it. If so, the original minimum (vertical) distance between them must be the depth of 27 km as estimated in the present study. This change of the distance from the initial value to the present one further suggests that, during the subsequent

subduction and exhumation history, the whole Iratsu body must have undergone an unrealistically strong tectonic shortening from >27 to 3 km (down to <1/9), i.e., a strain ratio X/Z of >81 if constant volume plane strain is assumed, where X and Z are length of stretching and shortening axes of strain ellipsoid, respectively. Strain analyses show that, even including rare samples recording unusually high and/or constrictional strains, X/Z (or R_f) values recognized for the Sambagawa schists are generally smaller than 30 (e.g., Toriumi and Noda, 1986; Aoya, 2022), and normally up to 5.8 (Wallis, 1995; Moriyama and Wallis, 2002; Shimizu and Yoshida, 2004), both being significantly smaller than 81. These data indicate that the present-day adjacence of the two bodies has not been achieved by an overall ductile thinning but, alternatively, by displacements along some fault located between the two bodies. That is, the boundary between the Western and Eastern Iratsu bodies (Fig. 1b) is tectonic in origin.

Even in the case where both the two bodies had originally formed the same oceanic plate in the footwall side, for example, dip-parallel motion of some high-angle fault located between them might theoretically juxtapose them after a vertical displacement of >20 km. Such a vertical displacement, however, is unrealistically large for an intraplate fault in the framework of the plate tectonics, where internal part of each plate is nearly rigid and relative motion between plates are sub-horizontal, thus, major fault displacements especially those with vertical component exclusively occur around plate boundaries. These discussions imply that the tectonic boundary between the Eastern and Western Iratsu bodies should not be a within-plate fault but a plate-plate (or slab-plate) boundary fault. Since the Western Iratsu body is agreed to have formed a surface part of an oceanic plate in the footwall side it can, therefore, be deduced that the Eastern Iratsu body was originally a part of the neighboring hanging-wall plate.

If the gabbroic Eastern Iratsu body originated in a deep (~ 27 km) part of continental crust on the hanging-wall side, accordingly experienced the granulite-facies metamorphism at the depth and was, at ~ 120 Ma, located closely above the subduction interface, then, it is possible that the subsequently subducted Western Iratsu body on the slab surface reached and finally captured the above-located Eastern Iratsu body at depth of 27 km (or possibly greater) along the subduction boundary. Probably, the two bodies were juxtaposed by a process of destroying the hanging-wall material such as tectonic erosion, after that, the juxtaposed two bodies have together undergone further subduction and the eclogite-facies overprinting during 120-90 Ma (Aoki et al., 2020b) and then ascended toward the Earth's surface. In this case, their tectonic history can be accounted for without invoking any unrealistic deformations which seem necessary for the above oceanic crust origin model and, therefore, we conclude that gabbroic protolith of the Eastern Iratsu body originated in the hanging-wall side, that is, in a deeper part of a continental arc and not in an oceanic island arc or other intra-oceanic edifices.

Near the eastern margin of the Eastern Iratsu body, there is occurrence of several meter-scale marbles (Fig. 1b). Based on isotopic studies yielding significantly low value of $\delta^{13}C$ (−5.1‰ relative to VPDB), Wada et al. (1984) suggest these marbles originated in relation with magmatic activity of gabbro formation. Using titanite and zircon in the Eastern-Iratsu marble, Yoshida et al. (2021) performed detailed petro-chronological studies including U-Pb spot dating and reported that the oldest metamorphic event of the marble closely after formation of the host gabbro occurred at ~ 200 Ma and was associated with P-T conditions of 2.3-2.7 GPa and 1000-1200 °C. The absolute values of the very high P-T estimates may not be very trustable possibly because of the unverified assumption of TiO_2 activity (0.5-0.8) in use of Zr-in-titanite thermometer without rutile (Hayden et al., 2008), however, on the other hand, it will be safe to consider the pressure condition was at least as high as 0.8 GPa as estimated in this study. Based on the high-P conditions of the 200-180 Ma event, Yoshida et al. (2021) suggest that the Eastern-Iratsu marble originated in the continental crust, the hanging-wall side of the subduction zone. As also pointed out by them, 200-180 Ma igneous activities are recognized in the Hida belt (e.g., Takahashi et al., 2018), which almost certainly formed the hanging-wall side at ~ 120 Ma. Endo et al. (2024), in their Figure 4, suppose that the Higo metamorphic terrane having similar chronological features with the Iratsu and Tonaru bodies (e.g., Dunkley et al., 2008; Suga et al., 2017; Osanai et al., 2021) formed a part of the hanging wall to the Late-Cretaceous Sambagawa subduction zone.

CONCLUSIONS

Pressure condition of 0.8 GPa was obtained for the granulite-facies metamorphism of the Eastern Iratsu body, which occurred during sometime between 200 and 120 Ma. This relatively high-pressure value can be interpreted to reflect metamorphic pressure in the lower continental crust of the hanging-wall side in the subduction zone. After this metamorphism, the Western Iratsu body, which was located near the footwall surface, initiated subduction at ~ 120 Ma and subsequently juxtaposed with the Eastern Iratsu body at the corresponding depth (~ 27 km or greater) along the subduction boundary, and then they

commonly underwent the eclogite-facies metamorphism by ~ 90 Ma. This means that the boundary between the Eastern and Western Iratsu bodies (Fig. 1b) is tectonic in origin and formed as fault or shear zone during 120–90 Ma. Thus, the eclogite-facies unit records not only subduction of the ocean-floor materials but also that of hanging-wall material. This indicates that tectonic erosion and dragging-down of the hanging-wall material by downgoing slab was at least in part active in the Sambagawa subduction zone environments.

ACKNOWLEDGMENTS

The thin section of the studied sample was made by T. Fujiwara, and constructive comments to this study were given by T. Nozaka in a seminar in Okayama University. Before starting this study, a precious sample from the Western Iratsu body was provided by S. Endo in Shimane University for understanding the metamorphic history of the Western Iratsu body. Valuable comments were also provided by two anonymous reviewers, and editorial works were performed by Y. Kouketsu in Nagoya University. We deeply appreciate these researchers and the technical staff in Okayama University for their cooperations.

REFERENCES

Aoki, K., Kitajima, K., Masago, H., Nishizawa, M., et al. (2009) Metamorphic P-T-time history of the Sanbagawa belt in central Shikoku, Japan and implications for retrograde metamorphism during exhumation. Lithos, 113, 393–407.

Aoki, S., Aoki, K., Chiba, K., Sakata, S., et al. (2020a) Origin of the Tonaru body in the Sanbagawa metamorphic belt, SW Japan. Island Arc, 29, e12332.

Aoki, S., Aoki, K., Tsujimori, T., Sakata, S. and Tsuchiya, Y. (2020b) Oceanic-arc subduction, stagnation, and exhumation: zircon U-Pb geochronology and trace-element geochemistry of the Sanbagawa eclogites in central Shikoku, SW Japan. Lithos, 358–359, 105378.

Aoya, M. (2002) Structural position of the Seba eclogite unit in the Sambagawa belt: supporting evidence for an eclogite nappe. Island Arc, 11, 91–110.

Aoya, M. (2022) Overprint of secondary Du folding in the Sambagawa metamorphic belt, SW Japan: Implications for strain ellipsoids and Paleogene tectonics of the east-Eurasian margin. Island Arc, 31, e12463.

Aoya, M., Tsuboi, M. and Wallis, S.R. (2006) Origin of eclogitic metagabbro mass in the Sambagawa belt: geological and geochemical constraints. Lithos, 89, 107–134.

Aoya, M., Endo, S., Mizukami, T. and Wallis, S.R. (2013a) Paleomantle wedge preserved in the Sambagawa high-pressure metamorphic belt and the thickness of forearc continental crust. Geology, 41, 451–454.

Aoya, M., Noda, A., Mizuno, K., Mizukami, T., et al. (2013b) Geology of the Niihama District. With Geological Sheet Map at 1:50000. pp. 181, Geological Survey of Japan, AIST (in Japanese with English abstract).

Aoya, M. and Endo, S. (2017) Recognition of the 'early' Sambagawa metamorphism and a schematic cross-section of the Late-Cretaceous Sambagawa subduction zone. Journal of the Geological Society of Japan, 123, 677–698 (in Japanese with English abstract).

Banno, S., Yokoyama, K., Iwata, O. and Terashima, S. (1976) Genesis of the epidote amphibolite units in the Sambagawa belt of central Shikoku. Journal of the Geological Society of Japan, 82, 199–210 (in Japanese with English abstract).

Dunkley, D.J., Suzuki, K., Hokada, T. and Kusiak, M.A. (2008) Contrasting ages between isotopic chronometers in granulites: monazite dating and metamorphism in the Higo Complex, Japan. Gondwana Research, 14, 624–643.

Endo, S. (2010) Pressure-temperature history of titanite-bearing eclogite from the Western Iratsu body, Sanbagawa Metamorphic Belt, Japan. Island Arc, 19, 313–335.

Endo, S., Wallis, S., Hirata, T., Anczkiewicz, R., et al. (2009) Age and early metamorphic history of the Sanbagawa belt: Lu-Hf and P-T constraints from the Western Iratsu eclogite. Journal of Metamorphic Geology, 27, 371–384.

Endo, S., Wallis, S.R., Tsuboi, M., Aoya, M. and Uehara, S. (2012) Slow subduction and buoyant exhumation of the Sanbagawa eclogite. Lithos, 146–147, 183–201.

Endo, S. and Tsuboi, M. (2013) Petrogenesis and implications of jadeite-bearing kyanite eclogite from the Sanbagawa belt (SW Japan). Journal of Metamorphic Geology, 31, 647–661.

Endo, S., Kouketsu, Y. and Aoya, M. (2024) Sanbagawa Subduction: What Went in, How Deep, and How Hot did it Get? Elements, 20, 77–82.

Goto, A. and Banno, S. (1990) Hydration of basic granulite to garnet-epidote amphibolite in the Sanbagawa metamorphic belt, central Shikoku, Japan. Chemical Geology, 85, 247–263.

Harley, S.L. (1984) An experimental study of the partitioning of Fe and Mg between garnet and orthopyroxene. Contributions to Mineralogy and Petrology, 86, 359–373.

Harley, S.L. and Green, D.H. (1982) Garnet-orthopyroxene barometry for granulites and peridotites. Nature, 300, 697–701.

Hayden, L.A., Watson, E.B. and Wark, D.A. (2008) A thermobarometer for sphene (titanite). Contributions to Mineralogy and Petrology, 155, 529–540.

Higashino, T. (1990) Metamorphic zones of the Sambagawa metamorphic belt in central Shikoku, Japan. Journal of the Geological Society of Japan, 96, 703–718 (in Japanese with English abstract).

Holland, T.J.B. and Powell, R. (1998) An internally consistent thermodynamic data set for phases of petrological interest. Journal of Metamorphic Geology, 16, 309–343.

Konzett, J. and Hoinkes, G. (1996) Paragonite-hornblende assemblage and their petrological significance: an example from the Austroalpine Schneeberg Complex, Southern Tyrol, Italy. Journal of Metamorphic Geology, 14, 85–101.

Kouketsu, Y., Enami, M., Mouri, T., Okamura, M. and Sakurai, T. (2014) Composite metamorphic history recorded in garnet porphyroblasts of Sambagawa metasediments in the Besshi region, central Shikoku, Southwest Japan. Island Arc, 23, 263–280.

Kugimiya, Y. and Takasu, A. (2002) Geology of the Western Iratsu mass within the tectonic mélange zone in the Sambagawa metamorphic belt, Besshi district, central Shikoku, Japan. Journal of the Geological Society of Japan, 108, 644–662 (in Japanese with English abstract).

Leake, B.E., Woolley, A.R., Arps, C.E.S., Birch, W.D., et al. (1997) Nomenclature of amphiboles: report of the subcommittee on amphiboles of the international mineralogical association, commission on new minerals and mineral names. Canadian Mineralogist, 35, 219–246.

Lee, H.Y. and Ganguly, J. (1988) Equilibrium compositions of coexisting garnet and orthopyroxene: experimental determinations in the system FeO–MgO–Al_2O_3–SiO_2, and applications. Journal of Petrology, 29, 93–113.

Miyagi, Y. and Takasu, A. (2005) Prograde eclogites from the Tonaru epidote amphibolite mass in the Sambagawa Metamorphic Belt, central Shikoku, southwest Japan. Island Arc, 14, 215–235.

Miyazaki, T., Nakamura, D., Tamura, A., Svojtka, M., et al. (2016) Evidence for partial melting of eclogite from the Moldanubian Zone of the Bohemian Massif, Czech Republic. Journal of Mineralogical and Petrological Sciences, 111, 405–419.

Molina, J.F. and Poli, S. (1998) Singular equilibria in paragonite blueschists, amphibolites and eclogites. Journal of Petrology, 39, 1325–1346.

Moriyama, Y. and Wallis, S. (2002) Three-dimensional finite strain analysis in the high-grade part of the Sanbagawa Belt using deformed meta-conglomerate. Island Arc, 11, 111–121.

Nakamura, D. (2003) Stability of phengite and biotite in eclogites and characteristics of biotite- or orthpyroxene-bearing eclogites. Contributions to Mineralogy and Petrology, 145, 550–567.

Osanai, Y., Kitano, I., Nakano, N., Adachi, I., et al. (2021) LA-ICP-MS zircon U-Pb ages of the Oshima metamorphic complex from Yawatahama-Oshima island and its geotectonic correlation. Journal of the Geological Society of Japan, 127, 1–24 (in Japanese with English abstract).

Ota, T., Terabayashi, M. and Katayama, I. (2004) Thermobaric structure and metamorphic evolution of the Iratsu eclogite body in the Sanbagawa belt, central Shikoku, Japan. Lithos, 73, 95–126.

Sakurai, T. and Takasu, A. (2009) Geology and metamorphism of the Gazo mass (eclogite-bearing tectonic block) in the Sambagawa metamorphic belt, Besshi district, central Shikoku, Japan. Journal of the Geological Society of Japan, 115, 101–121 (in Japanese with English abstract).

Sen, S.K. and Bhattacharya, A. (1984) An orthopyroxene-garnet thermometer and its application to the Madras charnockites. Contributions to Mineralogy and Petrology, 88, 64–71.

Shimizu, I. and Yoshida, S. (2004) Strain geometries in the Sanbagawa Metamorphic Belt inferred from deformation structures in metabasite. Island Arc, 13, 95–109.

Spear, F.S. (1993) Metamorphic phase equilibria and pressure-temperature-time path. pp. 799, Mineralogical Society of America, Washington, D.C.

Suga, K., Yui, T.-F., Miyazaki, K., Sakata, S., et al. (2017) A revisit to the Higo terrane, Kyushu, Japan: The eastern extension of the North China-South China collision zone. Journal of Asian Earth Sciences, 143, 218–235.

Takahashi, Y., Cho, D.-L., Mao, J., Zhao, X., et al. (2018) SHRIMP U-Pb zircon ages of the Hida metamorphic and plutonic rocks, Japan: Implications for late Paleozoic to Mesozoic tectonics around the Korean Peninsula. Island Arc, 27, e12220.

Takasu, A. (1984) Prograde and retrograde eclogites in the Sambagawa metamorphic belt, Besshi district, Japan. Journal of Petrology, 25, 619–643.

Takasu, A. (1989) P-T histories of peridotite and amphibolite tectonic blocks in the Sambagawa metamorphic belt, Japan. In Evolution of metamorphic belts (Daly, J.S., Cliff, R.A. and Yardley, B.W.D. Eds.). Geological Society, London, Special Publications, 43, 533–538. https://doi.org/10.1144/GSL.SP.1989.043.01.51

Tanaka, C. (1994) Electron microprobe analyses of rock-forming minerals from the eastern Iratsu epidote amphibolite mass in the Sambagawa metamorphic belt, central Shikoku, Japan. Geological Report of Shimane University, 13, 13–21.

Terabayashi, M., Okamoto, K., Yamamoto, H., Kaneko, Y., et al. (2005) Accretionary complex origin of the mafic-ultramafic bodies of the Sanbagawa belt, central Shikoku, Japan. International Geology Review, 47, 1058–1073.

Toriumi, M. and Noda, H. (1986) The origin of strain patterns resulting from contemporaneous deformation and metamorphism in the Sambagawa metamorphic belt. Journal of Metamorphic Geology, 4, 409–420.

Utsunomiya, A., Jahn, B.-m., Okamoto, K., Ota, T. and Shinjoe, H. (2011) Intra-oceanic island arc origin for Iratsu eclogites of the Sanbagawa belt, central Shikoku, southwest Japan. Chemical Geology, 280, 97–114.

Wada, H., Enami, M. and Yanagi, T. (1984) Isotopic studies of marbles in the Sanbagawa metamorphic terrain, central Shikoku, Japan. Geochemical Journal, 18, 61–73.

Wallis, S.R. (1995) Vorticity analysis and recognition of ductile extension in the Sanbagawa belt, SW Japan. Journal of Structural Geology, 17, 1077–1093.

Wallis, S. and Aoya, M. (2000) A re-evaluation of eclogite facies metamorphism in SW Japan: proposal for an eclogite nappe. Journal of Metamorphic Geology, 18, 653–664.

Whitney, D.L. and Evans, B.W. (2010) Abbreviations for names of rock-forming minerals. American Mineralogist, 95, 185–187.

Wood, B.J., Holland, T.J.B., Newton, R.C. and Kleppa, O.J. (1980) Thermochemistry of jadeite-diopside pyroxenes. Geochimica et Cosmochimica Acta, 44, 1363–1371.

Yokoyama, K. (1976) Finding of plagioclase-bearing granulite from the Iratsu epidote amphibolite mass in central Shikoku. Journal of the Geological Society of Japan, 82, 549–551.

Yokoyama, K. (1980) Nikubuchi peridotite body in the Sanbagawa metamorphic belt; Thermal history of the 'Al-pyroxene-rich suite' peridotite body in high pressure metamorphic terrain. Contributions to Mineralogy and Petrology, 73, 1–13.

Yoshida, K., Niki, S., Sawada, H., Oyanagi, R., et al. (2021) Discovery of the Early Jurassic high-temperature pre-Sanbagawa metamorphism recorded in titanite. Lithos, 398–399, 106349.

Manuscript received October 1, 2024
Manuscript accepted March 25, 2025
Advance online publication April 3, 2025
Released online publication April 24, 2025
Manuscript handled by Yui Kouketsu